THE EFFECT OF SIMPLE SHEAR ON STIFFNESS AND STRENGTH OF FABRIC LAMINATES

J. Hofstee [a] and F. van Keulen [b]

[a] *DLR - Institute of Structures and Design,*
Postfach 800320, D-70503 Stuttgart, Germany

[b] *Laboratory for Engineering Mechanics, Delft University of Technology,*
P.O. Box 5033, NL-2600 GA Delft, the Netherlands

SUMMARY: The effect of thermoforming induced simple shear on stiffness and strength of carbon plain weave reinforced laminates is investigated experimentally. Tensile tests are carried out in yarn direction, bias direction and an off-axis direction in which maximum shear coupling is expected. Obtained results are used to validate three classical laminate theory based stiffness models. The models take shear into account by defining equivalent uni-directional reinforced layers with identical properties and in-plane orientations as the yarns. Yarn crimp is either neglected or included with an isostrain or an isostress assumption. In yarn direction good agreement is found when crimp is included. In other directions agreement is less because the influence of resin pockets is neglected for all models. Strength is approximately constant in yarn direction and highly increases in bias direction for sheared laminates.

KEYWORDS: sheared fabric, yarn crimp, laminate stiffness, thermoforming, tensile test, anisotropy, plain weave

INTRODUCTION

Thermoforming techniques for Continuous Fibre Reinforced ThermoPlastic (CFRTP) laminates provide a cost effective method for manufacturing complex three dimensional (3D) shapes [1]. Common reinforcements are aramid, glass and carbon Woven Fabric (WF). During thermoforming, yarn orientations change as the fabric is draped over a 3D surface. These reorientations are dominated by pure shear deformations, also denoted as simple shear or Trellis effect [1–4]. For simple shear deformations, the inter yarn angle (θ) changes, while yarns are assumed not to slip at their crossover points, see Fig. 1. The simple shear deformation significantly affects laminate stiffnesses [2–4]. In recent work [5], it was shown that yarn crimp increases with shear and should be taken into account as well. Two Classical Laminate Theory (CLT) based stiffness models were developed that account for both simple shear and yarn crimp. Yarns were substituted by undulated Uni-Directional (UD) layers and pure resin material was substituted by an isotropic layer. Yarn layer properties were corrected for crimp by assuming either constant stress (isostress) or constant strain (isostrain). For both models, closed form expressions were obtained which require very little computational effort. Input consists of material properties, simple geometric measurements on an undeformed orthogonal WF laminate and the inter

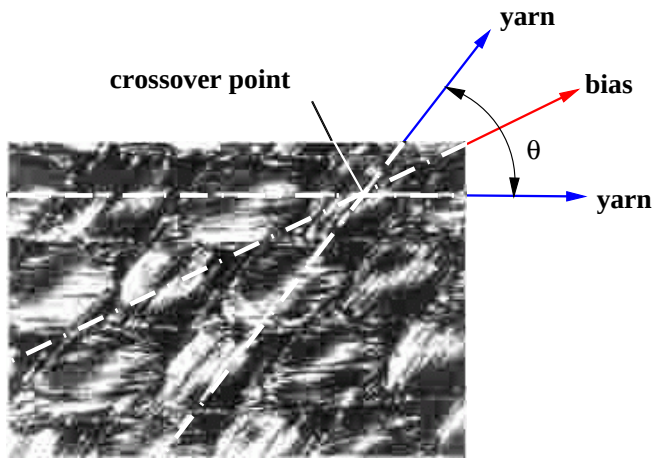

Fig. 1. Top view of a simple sheared carbon plain weave

yarn angle (θ) after thermoforming. Because fast predictions for the laminate stiffnesses are obtained as a function of θ only, the CLT isostress and isostrain models are suitable as a link between kinematic thermoforming simulations and Finite Element (FE) analyses.

To validate the proposed stiffness models, tests on sheared WF laminates are required. These types of experiment received little attention so far. Smith *et al.* [2] studied the effect of a simple shear deformation on Young's modulus and Poisson's ratio of several thermoset glass fabric laminates. Dry fabrics were sheared using a four-bar rig (also denoted as shear frame) and impregnated afterwards. Reasonable agreement was found with CLT predictions, regarding the yarns as non-crimped UD reinforced layers and the matrix as isotropic layers. All tests were carried out in bias direction, which is depicted in Fig. 1. It will be shown here that the effect of yarn crimp on stiffness is negligible in bias direction. Hofstee *et al.* [5] performed bending tests on specimens obtained from an actual thermoformed product reinforced with a carbon plain weave. Again, tests were carried out in bias direction. Reasonable agreement was found with the CLT isostress and isostrain models mentioned above. Test specimens in yarn direction and directions that exhibit shear coupling were not investigated. Furthermore, shear deformations were limited to $\theta \approx 70°$ whereas shear deformations up to $\theta \approx 50°$ can be expected in practice.

In the present work, tensile response of a plain WF reinforced laminate is investigated more thoroughly by performing tests in bias direction, yarn direction and directions for which maximum shear coupling is expected. Shear angles up to the locking angle are investigated. Furthermore, the effect of simple shear on tensile strength of the laminate is studied. Test specimens are manufactured with a shear frame. The paper is organized as follows. CLT isotress and isostrain models are repeated in a concise manner. The preparation of tensile test specimens with the shear frame is treated. Tensile test results are presented, and a comparison is made between CLT models and experiment. The error caused by conventional clamping devices on test specimens with anisotropic behaviour is taken into account. Finally, the CLT isostress and isostrain models are validated and an outlook is given.

THEORY

Laminate Stiffness Models for a Thermoformed Plain Woven Fabric Laminate

The half product used for all experiments is a Carbon Fibre / PolyPhenylene Sulfide (CF/PPS) plain weave reinforced laminate ($n = 6$). Laminate specifications are given in Table 1. This lam-

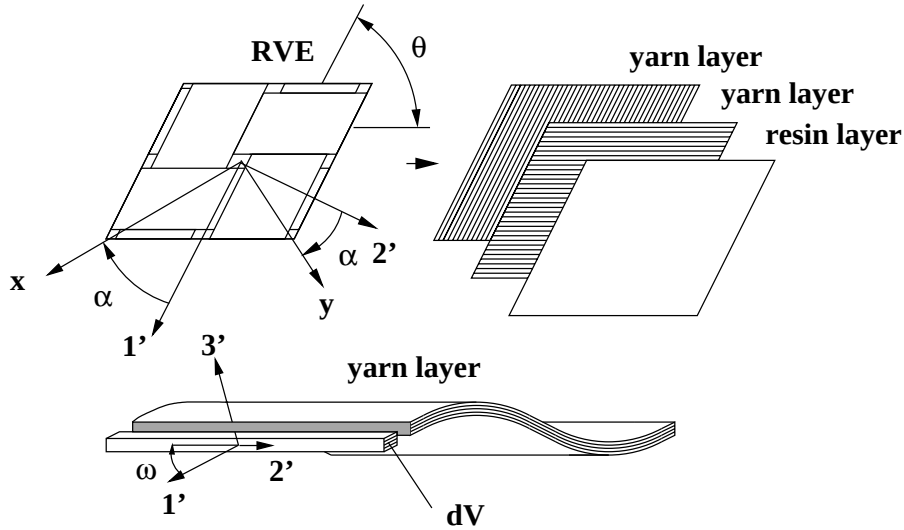

Fig. 2. Schematization of CLT laminate stiffness calculation using substitute layers for yarns and pure resin material

inate is chosen for the following reasons. Firstly, carbon fibres exhibit higher anisotropy than aramid or glass fibres. Secondly, yarns in a plain weave are crimped more than in other weave types like twill or satin. The effect of fibre reorientations on laminate stiffness is therefore expected to be more pronounced.

In-plane laminate stiffness calculation is carried out on Repeating Volume Elements (RVE) of every WF lamina (Fig. 2). In the present study, the analysis can be restricted to the RVE of a single lamina because all laminae have identical orientations and only in-plane stiffnesses are analyzed. For laminate stiffness calculation with CLT, the RVE is subdivided into two undulated UD reinforced layers representing the yarns, and one isotropic layer representing the pure resin material. Substitute layer thicknesses can easily be derived from laminate thicknesses and manufacturer's data [5]. In-plane layer orientations are taken identical to those of the yarns. For the undulated yarn layers the equivalent elastic properties are determined in their local transversely isotropic coordinate systems $(1', 2', 3')$ using the Composite Cylinder Assemblage micromechanics model [6]. Elastic properties of fibre and resin from Table 2 are used, and an intra yarn fibre volume fraction of $\phi_{\text{fib}} = 0.70$ is assumed. Next, the local yarn properties are transformed to global coordinates (x, y, z) with the x-axis corresponding to the test direction. To this effect, a coordinate transformation is carried out around the local crimp angle (ω) of the yarn element, and the angle α, see Fig. 2.

Table 1
Material specifications of the undeformed CF/PPS laminate

Stacking sequence		$[0_3]_S$
Laminate thickness	t^0_{lam} (mm)	1.30
Global fibre volume fraction	v_{fib} (%)	$48 - 52$
Fabric type		Ten Cate CD 206 balanced plain weave
Yarn type		3K Carbon T-300J
Yarn count	(no.yarns/10cm)	50
Resin film		Lipp-Terler Lite P PPS 25

Table 2
Elastic properties of fibres in longitudinal (subscript L) and transverse (subscript T) directions, and isotropic resin properties.

	E_L (GPa)	E_T (GPa)	ν_{LT} (-)	ν_{TT} (-)	G_{LT} (GPa)
Fibre	230	40.0	0.26	0.40	24.0
Resin	3.9		0.35		1.4

In [5], it is shown that the local crimp angle can be approximated as

$$\omega = f(a_b^{0^*}, A^{0^*}, \theta) \quad . \tag{1}$$

The first two parameters represent normalized bridged yarn width ($a_b^{0^*} = a_b^0/l^0$) and normalized undulation amplitude ($A^{0^*} = A^0/l^0$), see Fig. 3a. Superscript 0 indicates the undeformed laminate configuration, i.e. before thermoforming. Based on geometry analyses on a thermoformed product, it is observed in [5] that crimp increases with shear and can be written as a function of θ. Fig. 3b shows the maximum value of the crimp angle (Ω) as approximated for stiffness modeling. Good agreement is found with crimp angles measured on the sheared laminates used here.

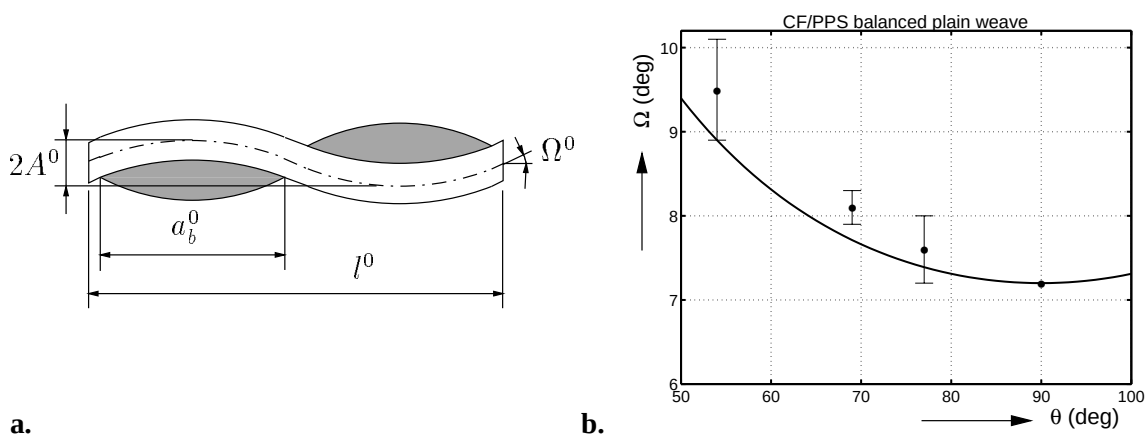

Fig. 3. a) Measurements on the undeformed fabric for definition of crimp. b) Maximum crimp angle (Ω) as a function of shear; model approximation versus experiment.

To account for crimp in laminate stiffness calculation, two approaches are presented:

- *CLT isostrain model* - Effective stiffnesses of the yarn layers are obtained by volume averaging of local yarn stiffnesses, i.e. constant strain is assumed.
- *CLT isostress model* - Effective compliances of the yarn layers are obtained by volume averaging of local yarn compliances, i.e. constant stress is assumed. Effective substitute layer stiffnesses are subsequently obtained by inverting the compliance matrix.

For the $[0_3]_s$ laminate, in-plane stiffnesses are obtained by straightforward application of CLT to the three substitute layers of a single RVE.

Choice of Test Directions

For comparison of the in-plane laminate response with model predictions, Young's modulus (E_x), Poisson's ratio (ν_{xy}) and shear coupling coefficients ($\eta_{xy,x}$) are measured for directions

in which extreme values are expected. For uniform global stresses $\sigma_x \neq 0, \sigma_y = \tau_{xy} = 0$, the engineering constants of a symmetric laminate are given by (see e.g. [7])

$$E_x = \frac{\sigma_x}{\epsilon_x} = \frac{1}{a^*_{11}} \quad ; \quad \nu_{xy} = -\frac{\epsilon_y}{\epsilon_x} = -\frac{a^*_{12}}{a^*_{11}} \quad ; \quad \eta_{xy,x} = \frac{\gamma_{xy}}{\epsilon_x} = \frac{a^*_{16}}{a^*_{11}} \quad . \tag{2}$$

Elements of the laminate compliance matrix ($\boldsymbol{a}^*$) are calculated with the CLT isostress and isostrain models as described in the preceding section. The engineering constants are shown as a function of test direction in Fig. 4 for the undeformed, and Fig. 5 for the maximum sheared laminate. The test direction is defined by the angle β between the x-axis and the bias direction with lower inter yarn angle (θ). Thus, $\beta = 0°$ and $\beta = 90°$ are the bias directions, whereas $\beta = \pm\theta/2$ are the yarn directions.

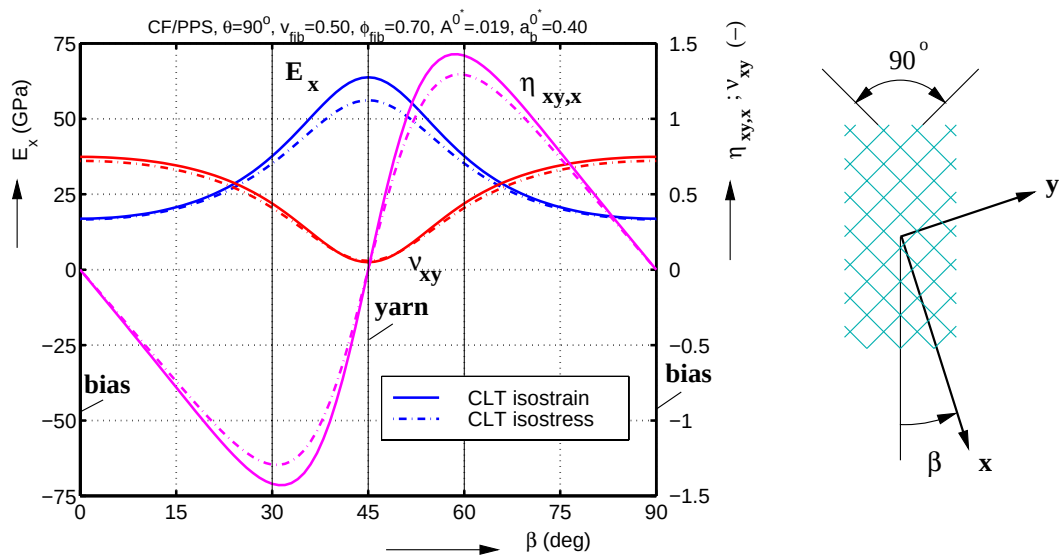

Fig. 4. Influence of test direction on engineering properties of the undeformed CF/PPS laminate.

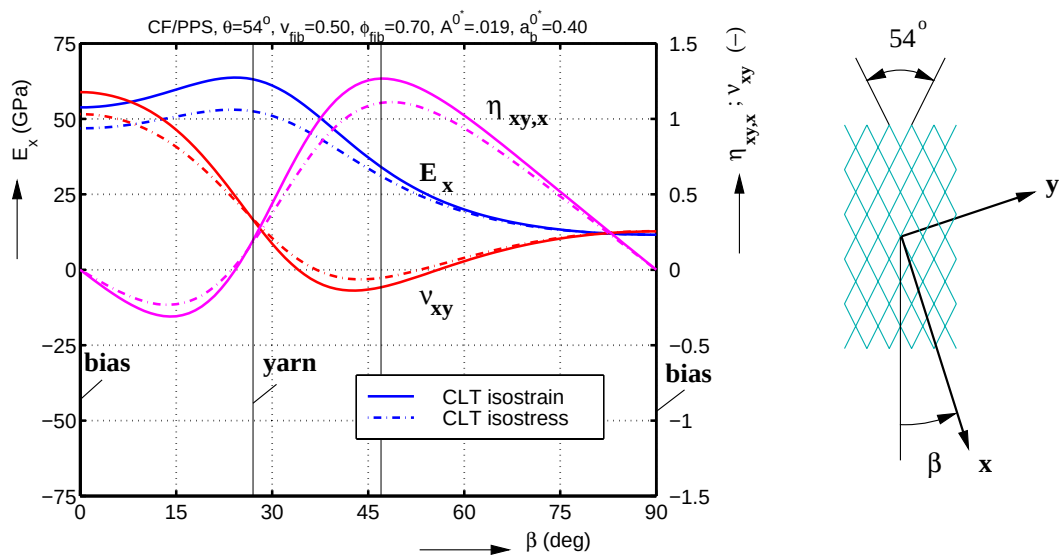

Fig. 5. Influence of test direction on engineering properties of the maximum sheared CF/PPS laminate.

It is seen from Figures 4 and 5 that Young's moduli are highest in yarn directions, and Poisson's ratios reach maximum values in the bias directions defined by $\beta = 0$. These two test directions are selected to validate the proposed stiffness models and to characterise the effect

of simple shear on E_x and ν_{xy}, respectively. Shear coupling is highest for $\beta \approx \theta/2 \pm 15°$ in the undeformed configuration and $\beta \approx \theta/2 + 20°$ in the maximum sheared configuration. Hence, off-axis specimens with $\beta = \theta/2 + 17°$ are chosen for validation of shear coupling predictions.

PREPARATION OF TEST SPECIMENS

To obtain a simple shear deformation, an orthogonal fabric reinforced laminate is clamped in a hinged shear frame (Fig. 6a). Subsequently, the clamped laminate is heated above melting temperature of the thermoplastic resin and sheared in an oven. Fig. 6b shows a number of laminates with varying shear deformations obtained with this procedure. It should be mentioned that the pattern visible on the front laminate is due to PPS oxidation. In the lower left and upper right corners small out-of-plane buckling regions are present. This buckling occurs because the part of the laminate clamped in the shear rig does not melt during the short heating cycle. After shearing, the laminate is taken out of the rig and re-consolidated. Finally, specimens are cut from the laminates.

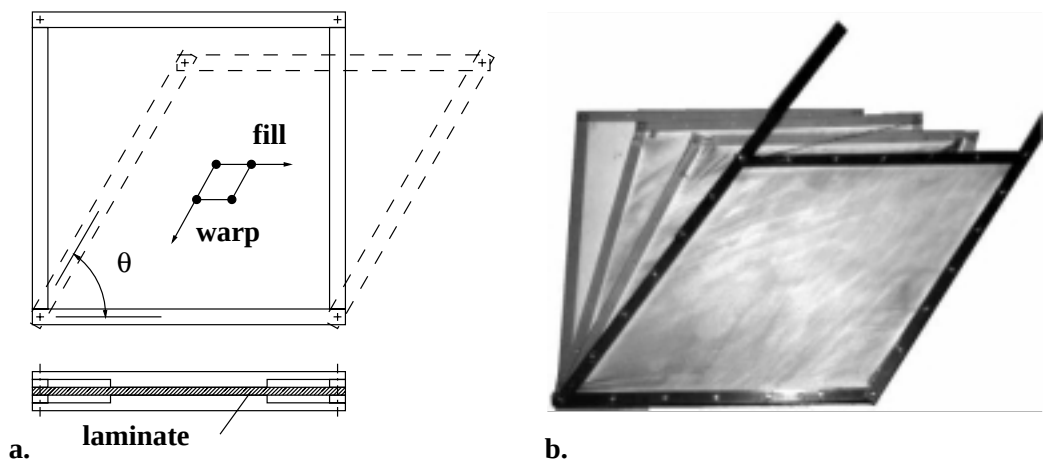

Fig. 6. a) Schematization of simple shear deformation mode and shear frame. b) Laminates after deformation in shear rig

The largest shear deformation obtained with the shear rig is $36°$ ($\theta = 54°$). Local variations in θ are verified visually and with photomicrograph analysis on laminate cross sections that are taken in both yarn directions on three locations for every laminate. For all specimens, variations in inter yarn angle are smaller than 2 degrees. The laminate cross section photomicrographs are used to verify laminate quality as well. No cracks or delaminations are detected and no voids are visible in regions where specimens are cut from the laminates. Global fibre volume fractions are determined for all test specimens individually and are not affected by shearing and re-consolidation.

Table 3
Specimen types

Direction	*Number of specimens*	*Overall dimensions (mm)*	*Length to width ratio*
Yarn	5	250x25	7.5
Bias	3	150x15	7.5
Off axis	3	250x25	7.5

Tensile tests are carried out on the sheared specimens according to ASTM D-3039. Specimens are conditioned and tested at room temperature and 50% relative humidity. The number of specimens and their dimensions are given in Table 3. Specimen thickness (t_{lam}) increases with shear (see [5]) and is approximated by

$$t_{\mathrm{lam}} = \frac{t^0_{\mathrm{lam}}}{\sin\theta} \quad . \tag{3}$$

A constant head displacement of 2mm/min is used for all specimens. Strain data in longitudinal direction are recorded with an extensometer with grip base distance of 50mm. Strain data in transverse and $\pm 45°$ directions are recorded with 6mm strain gages. For all weave configurations, gage lengths exceed the RVE dimensions in the direction of measurement, as recommended for triaxial braids by Masters and Ifju [8]. Differences between extensometer and gage results are within the data scatter for nearly all strain measurements in x-direction.

TENSILE TEST RESULTS

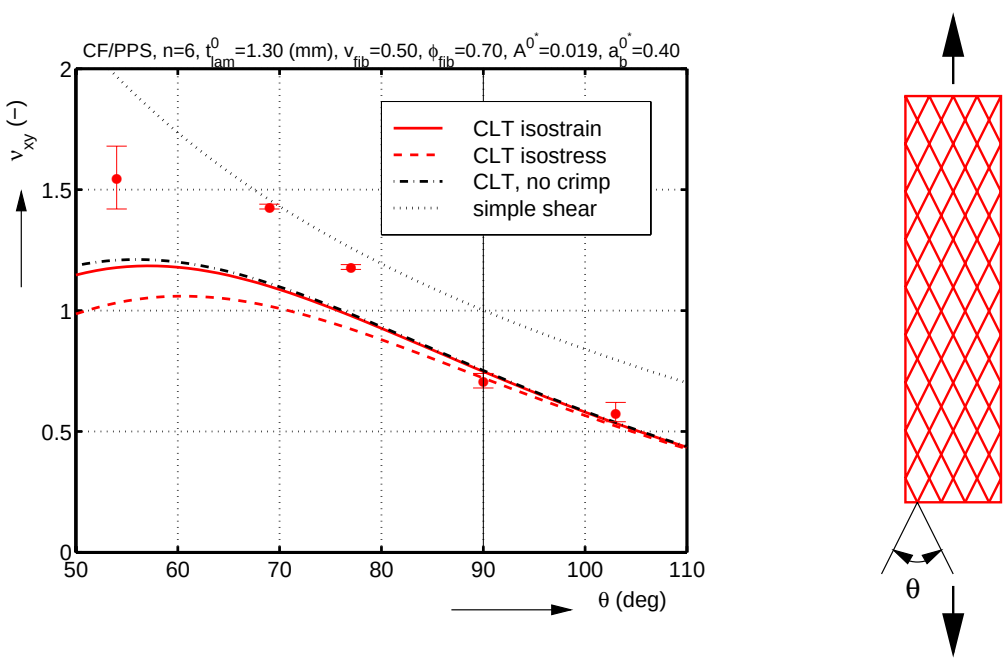

Fig. 7. Poisson's ratio (ν_{xy}) in bias direction as a function of the inter yarn angle (θ)

Poisson's ratios in bias direction of the sheared laminates are shown in Fig. 7. Predictions for ν_{xy} increase with decreasing θ and reach a maximum value at $\theta \approx 60°$. For small inter yarn angles (large shear deformations) the CLT isostress model yields lower predictions due to yarn crimp. Very good agreement with all models is found for $\theta > 90°$. Experiments for inter yarn angles $\theta < 90°$ give a significantly higher value than the model predictions. The differences between theory and experimental results correspond to those found for glass reinforced thermoset laminates by Smith *et al.* [2]. A major cause for these differences is that the CLT based models applied here idealize the material as UD cross-ply laminates, consequently neglecting pure resin pockets between the yarns. Due to the low shear modulus of the PPS matrix, these regions allow the fabric to deform similar to the pure kinematic simple shear deformation mode assumed for thermoforming deformations (Fig. 6a). It is seen from Fig. 7 that this can significantly increase Poisson's ratio in bias direction.

In yarn and off-axis directions, the shear coupling ($\eta_{xy,x}$) is nonzero as can be derived from Fig. 4 and Fig. 5. Conventional end clamps are used for tensile testing, and the specimens are constrained at these end clamps which induces a non-uniform state of stress. Herakovich [7] gives expressions for the error that is consequentially made when measuring engineering constants on the specimen centreline The ratio of apparent to actual engineering constants is given by

$$\frac{E_x}{\overline{E}_x} = \frac{1-\eta}{1-\frac{2}{3}\eta} \quad ; \quad \frac{\eta_{xy,x}}{\overline{\eta}_{xy,x}} = \frac{1-\eta}{1-\left(\frac{S_{11}S_{66}}{S_{16}^2}\right)\eta} \quad \text{with} \quad \eta = \frac{6\left(\frac{S_{16}}{S_{11}}\right)^2}{6\left(\frac{S_{66}}{S_{11}}\right)+\left(\frac{2L}{W}\right)^2} \quad , \tag{4}$$

with $\overline{E}_x$ and $\overline{\eta}_{xy,x}$ the apparent experimental engineering constants, E_x and $\eta_{xy,x}$ the actual engineering constants and (L/W) the specimen length to width ratio between the clamps. Actual compliances S_{ij} are estimated with the CLT model neglecting crimp. The relations are applied to correct the experimental results. A significant difference is found for the shear coupling ratios only.

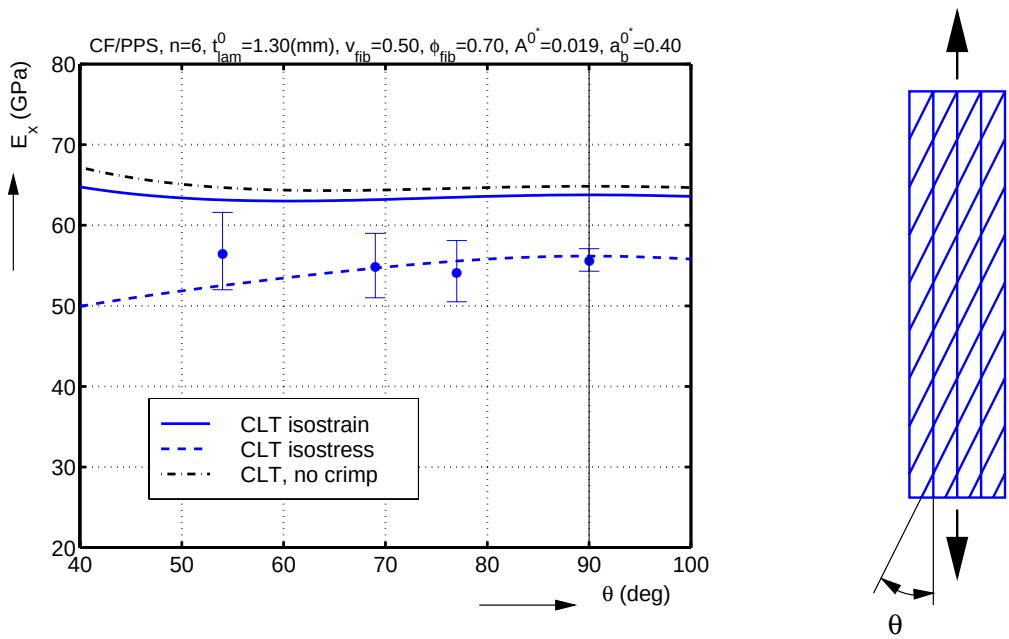

Fig. 8. Young's modulus (E_x) in yarn direction as a function of the inter yarn angle (θ)

Fig. 8 shows measured and predicted Young's modulus in yarn direction as a function of θ. Due to the anisotropy of the yarns, predictions for Young's moduli are affected only slightly by shear for the shown range of θ. The stiffness model neglecting crimp [2] gives the highest predictions. Isostrain model predictions differ only slightly, but isostress model predictions are significantly lower due to yarn crimp. Yarn crimp increases with shear (Fig. 3b) and consequently the difference between isostrain and isostress models slightly increases with decreasing inter yarn angle (for $\theta < 90°$). For small shear deformations, experimental results correspond well with the isostress predictions. For $\theta = 54°$ the experimental value lies between isostress and isostrain predictions. A cause for this apparent increase in stiffness may be that yarn straightening is more restricted for a laminate with θ close to the locking angle.

Fig. 9 shows analytical and experimental results for the shear coupling coefficient. Shear coupling is maximum at an inter-yarn angle of $\theta \approx 80°$. It should however be noted that the in-

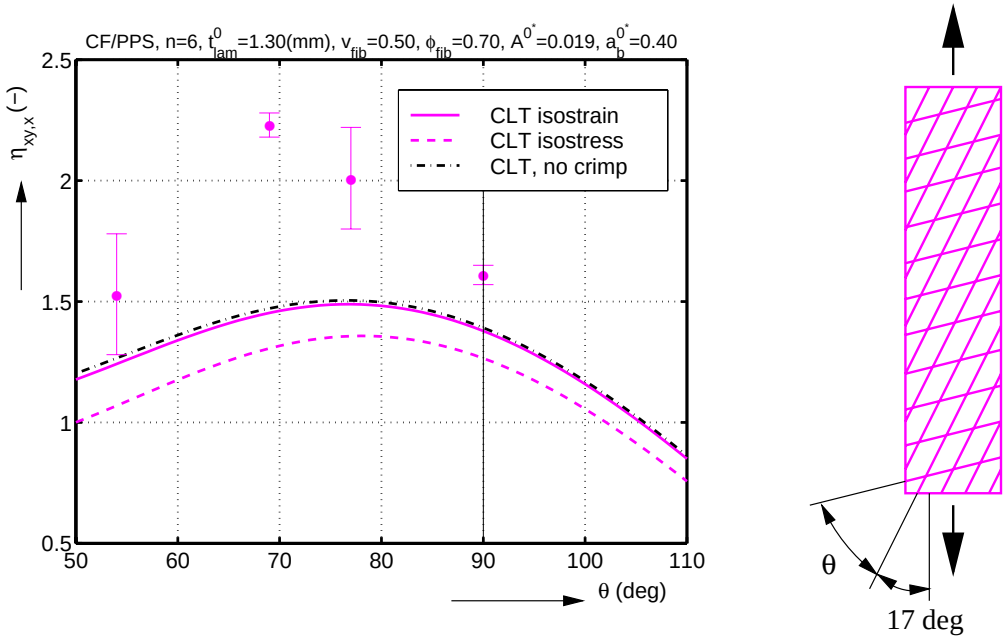

Fig. 9. Shear coupling ratio $(\eta_{xy,x})$ in 17 degrees off (yarn-)axis direction as a function of the inter yarn angle (θ)

dicated 17° off-axis direction represents the direction with maximum shear coupling only in approximation (Fig. 4 and Fig. 5). Experimental results are significantly higher for all shear deformations. A cause for this may once more be the presence of pure resin pockets. Correction factors for conventional clamps are up to $\eta_{xy,x}/\overline{\eta}_{xy,x} = 1.29$. For more reliable results, specimens with higher length to width ratio should therefore be tested.

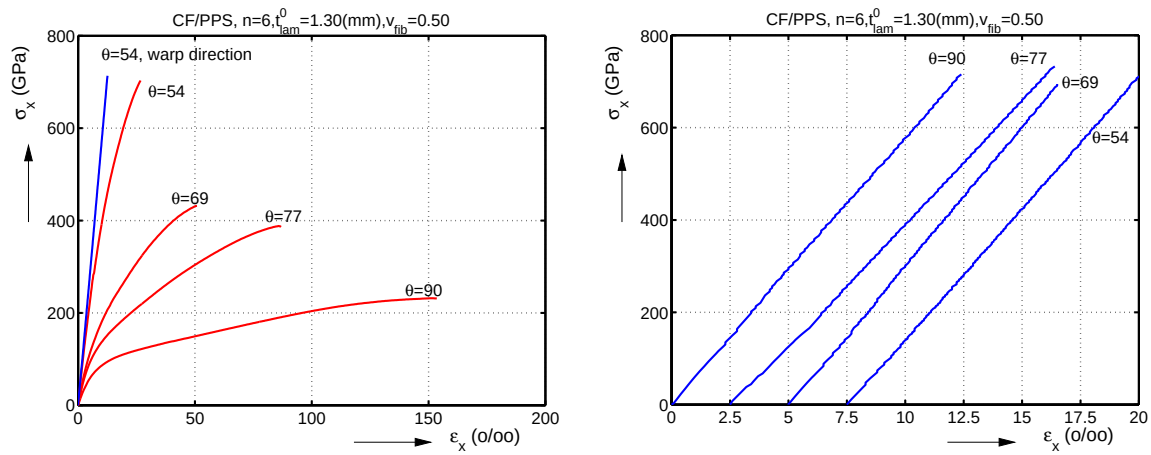

a. **b.**

Fig. 10. Representative tensile responses for various angles θ. a) Bias direction. b) Yarn direction.

Tensile responses in yarn and bias directions are shown in Fig. 10a and b, respectively. In bias direction highly nonlinear response is observed and in yarn direction the stress-strain relation is approximately linear. This is due to the fact that nonlinear material behavior of the resin dominates in bias direction, whereas linear material behavior of the fibres dominates in yarn direction. Strength in yarn direction appears to be independent of θ. Ultimate stresses are approximately $\sigma_{\mathrm{ult}} = 700$MPa for all laminates (Fig. 10b). Thermoforming induced shear deformations affect tensile strength in bias direction significantly. Observed ultimate stress increases from $\sigma_{\mathrm{ult}} = 232$MPa for the orthogonal configuration to $\sigma_{\mathrm{ult}} = 721$MPa,i.e. comparable to strength in yarn direction, for $\theta = 54^\circ$ (Fig. 10a).

CONCLUSIONS

Tensile tests were presented to validate three CLT based stiffness models for simple sheared WF laminates. Based on experimental results for the CF/PPS laminate Young's modulus in yarn direction, the CLT isostress model including yarn crimp is considered to yield the most reliable results. Poisson's ratios were measured in bias direction and shear coupling coefficients were measured in an off-axis direction where high values were expected. Although the trend as a function of inter yarn angle was reasonably predicted, all three CLT based models yielded significantly lower predictions. A cause for this was assumed to be the effect of pure resin pockets which exhibit low shear moduli. These resin pockets are neglected by the CLT based models, and more rigorous modeling is required for accurate predictions.

Experimental results are given for stress-strain responses in bias and yarn direction. Stress-strain responses in bias direction were highly nonlinear. In yarn direction, the influence of the thermoforming induced simple shear deformation on ultimate strength is negligible. In bias direction, ultimate strength of the sheared CF/PPS laminate with $\theta = 54°$ is more than three times that of the undeformed laminate ($\theta = 90°$).

ACKNOWLEDGEMENTS

Ten Cate Advanced Composites and the Max Planck Gesellschaft are gratefully acknowledged for their contributions to the present work.

REFERENCES

[1] Bergsma, O.K., "Three dimensional simulation of fabric draping, development and application", *Proceedings of the Ninth International Conference on Composite Materials,*, Madrid, Spain, July 12–16, 1993, Vol.IV, Miravete, A., Ed., pp. 560–567.

[2] Smith, P., Rudd, C.D. and Long, A.C., "The effect of shear deformation on the processing and mechanical properties of aligned reinforcements", *Composites Science and Technology* , Vol. 57, 1997, pp. 327–344.

[3] Vu-Khanh, T. and Liu, B., "Prediction of fibre rearrangement and thermal expansion behaviour of deformed woven-fabric laminates", *Composites Science and Technology* , Vol. 53, 1995, pp. 183–191.

[4] van West, B.P., Pipes, R.B. and Keefe, M., "A simulation of the draping of bidirectional fabrics over arbitrary surfaces", *Journal of the Textile Institute* , Vol. 81, 1990, pp. 448–460.

[5] Hofstee, J., van Keulen, F., de Boer, H. and Stellbrink, K., "Stiffness analysis of thermoformed plain weave composites", *Proceedings of the Eighth European Conference on Composite Materials*, Naples, Italy, June 3–6, 1998, Vol. II, Crivelli-Visconti, I., Ed., pp. 651–658.

[6] Hashin, Z., "Analysis of composite materials - a survey", *Journal of Applied Mechanics*, Vol. 50, 1983, pp. 481–505.

[7] Herakovich, C.T., *Mechanics of Fibrous Composites*, John Wiley & Sons, Inc., New York, 1998.

[8] Masters, J.E. and Ifju, P.G., "Strain gage selection criteria for textile composite materials", *Journal of Composites Technology & Research, JCTRER*, Vol. 19, No. 3, 1997, pp. 152–167.

[9] Pagano, N.J. and Halpin, J.C., "Influence of end constraint in the testing of anisotropic bodies", *Journal of Composite Materials*, Vol. 2, No. 1, 1968, pp. 18–31.